International Journal of Hydrogen Energy 84 (2024) 593–605

Contents lists available at ScienceDirect

International Journal of Hydrogen Energy

journal homepage: www.elsevier.com/locate/he

# Fuzzy logic-based coordinated operation strategy for an off-grid photovoltaic hydrogen production system with battery/supercapacitor hybrid energy storage

Xiaolun Fang [a], Xinyu Zhong [a], Wei Dong [a], Fan Zhang [a,*], Qiang Yang [b]

[a] School of Automation, Hangzhou Dianzi University, Hangzhou, 310018, China
[b] College of Electrical Engineering, Zhejiang University, Hangzhou, 310027, China

ARTICLE INFO

Handling editor: Mehran Rezaei

*Keywords:*
Coordinated operation strategy
Photovoltaic-based hydrogen production system
Fuzzy logic control
State of charge feedback

ABSTRACT

The coupling of photovoltaic power generation with water electrolyzer is advantageous for enhancing solar energy utilization and generating green hydrogen. In this work, an off-grid photovoltaic-based hydrogen production system consisting of photovoltaic, electrolyzer, battery energy storage system and supercapacitor was developed. A coordinated operation strategy is designed to manage the power of each unit in the system to avoid significant fluctuations in working power and frequent start-stop operations of the electrolyzer unit. Firstly, the coordinated operation strategy sets five operation modes for the photovoltaic-based hydrogen production system, and the fuzzy logic control algorithm is used to choose the operation mode to determine the reference power of each unit. On this basis, the state of charge feedback-based first-order low-pass filter algorithm is used to achieve the power allocation to mitigate deep charging and discharging of the supercapacitor. The proposed solution is extensively assessed through comparative simulation experiments based on three typical test days. The numerical results confirm its effectiveness and demonstrate the potential for achieving high system efficiency.

Nomenclature

| | |
|---|---|
| ***Indices*** | |
| $t$ | Time slot index |
| ***Parameters and Constants*** | |
| $P_{EL}^{min}$/ $P_{EL}^{max}$ | Lower/upper boundary of the power input of the EL unit (kW) |
| $E_{EL}$ | Energy conversion factor |
| $\eta_{EL}$ | Efficiency of the EL unit (%) |
| $\eta_{type,ch}$/ $\eta_{type,disc}$ | Efficiency of the power charging and discharging (%) |
| $C_{type}$ | Energy storage capacity (kWh) |
| $SOC_{type}^{min}$/ $SOC_{type}^{max}$ | Upper/lower limit of the SOC value |
| $P_{type,ch}^{max}$/ $P_{type,disc}^{max}$ | Maximum power charging/discharging power (kW) |
| $\alpha$ | Filtering coefficient |
| $a$/ $b$ | Filter coefficient corresponding to the EL/BESS |
| $\tau$ | Time constant of the filter |
| $T_s$ | Sampling time (s) |
| $e_{EL}$ | Coefficients of EL start-stop cost |
| $d_{EL}$ | Coefficients of EL power fluctuation cost |

(*continued on next column*)

(*continued*)

| | |
|---|---|
| ***Variables*** | |
| $H_{EL}$ | Hydrogen produced by the EL unit (kg) |
| $P_{EL}$ | Electricity consumed by the EL unit (kW) |
| $P_{type,ch}$/ $P_{type,disc}$ | Charging/discharging power (kW) |
| $P_{EL}^{*}$/ $P_{BESS}^{*}$ | Reference power instructions for the EL/BESS unit (kW) |
| $P_i$/ $P_o$ | Input/output power signal of the filter |
| $P_{PV}$ | PV power output (kW) |
| $P_{BESS}$ | Power values of the BESS unit (kW) |
| $P_{SC}$ | Power values of the SC unit (kW) |
| $P_{EL-L}^{*}$/ $P_{EL-H}^{*}$ | Low-frequency/high-frequency component of the reference power instructions for the EL (kW) |
| $P_{BESS-L}^{*}$/ $P_{BESS-H}^{*}$ | Low-frequency/high-frequency components of the reference power instructions for the BESS (kW) |
| $\sigma_{EL}^{on}$/ $\sigma_{EL}^{off}$ | Number of start-up/shutdown times of the EL unit |
| $\Delta P_{EL}$ | Power fluctuation of the EL unit (kW) |
| ***Abbreviation*** | |
| EL | Electrolyzer |
| PEM-EL | Polymer exchange membrane electrolyzer |
| PV | Photovoltaic |

(*continued on next page*)

* Corresponding author.
*E-mail address:* zhangfan@hdu.edu.cn (F. Zhang).

https://doi.org/10.1016/j.ijhydene.2024.08.188
Received 16 April 2024; Received in revised form 1 August 2024; Accepted 11 August 2024
Available online 21 August 2024

(*continued*)

| | |
|---|---|
| BESS | Battery energy storage system |
| SC | Supercapacitors |
| SOC | State of charge |
| FLF | First-order low-pass filter |

## 1. Introduction

Currently, hydrogen energy has emerged as a promising option for future energy systems, offering the advantages of high energy density, easy storage, and zero carbon emission [1]. Hydrogen production methods mainly consist of fossil fuel-based hydrogen processes, biomass-based approaches and electrolysis-based techniques, and electrolysis-based hydrogen production is recognized for its low carbon and high purity [2]. Since electricity costs account for about 80% of the total cost of hydrogen production through the electrolyzer (EL), the choice of energy source is crucial. Although renewable energy sources like wind and solar require initial investments in equipment installation and maintenance, they offer very low electricity production costs once operational. Consequently, utilizing renewable energy can substantially reduce the cost of hydrogen production. Integrating a renewable energy generation system with the EL provides an economically viable method for producing green hydrogen while also enhancing the utilization of renewable energy [3]. The polymer exchange membrane electrolyzer (PEM-EL) has attracted extensive attention due to its fast response speed making it suitable for intermittent and fluctuating renewable energy generation [4].

The coupling of photovoltaic (PV) and EL can be divided into direct coupling mode and indirect coupling mode [5,6]. In the direct coupling mode, the PV array is directly connected to the EL without the need for intermediary storage devices, making the system simpler and less costly. The indirect coupling mode involves additional components such as battery energy storage systems (BESS), which act as intermediaries between the PV array and the EL, facilitating enhanced energy management and system efficiency.

Some studies on the direct coupling of PV and EL have been reported. In Ref. [7], the direct coupling hydrogen production technology between PV modules and ELs was studied by converting the I–V output characteristics of the PV array into the input characteristics of the EL. This allows for the optimal operation of both modules, maximizing hydrogen production using PV electricity. In Ref. [8], the authors designed a renewable energy hydrogen production system that directly couples the EL with a hybrid wind-solar power generation system, and utilized the imperialist competitive algorithm to maximize hydrogen production and reduce the curtailment of wind and solar energy. In Ref. [9], an AC-linked PV-PEM system was proposed, and the solar plant-to-EL capacity ratio was used as the optimization variable. The findings revealed that when optimized to minimize the cost of hydrogen, this ratio was approximately 54%. The direct coupling mode eliminates the need for auxiliary equipment, which reduces the cost and complexity of the entire system [10]. However, the mismatch between the PV array and the EL unit may result in significant energy losses. Additionally, in this coupling mode, the EL unit needs to absorb intermittent and fluctuating power, resulting in frequent start-stop and significant working power fluctuations, which can potentially degrade the EL and impact its lifetime [11].

Indirect PV-EL coupling is another common configuration that incorporates auxiliary components such as BESS, which serve as intermediaries between the PV array and the EL unit. This configuration ensures the reliable consumption of renewable energy and efficient operation of hydrogen production [12]. Through strategic management of the BESS, this configuration provides a stable power supply to the EL, effectively mitigating the impact of photovoltaic (PV) intermittency on the frequent start-stop cycles of the EL and reducing the rate of degradation of the EL equipment. In Ref. [13], the authors utilized a BESS to absorb the output of a hybrid wind-solar power generation system and subsequently supplied it to an EL unit for hydrogen production. An off-grid PV hydrogen production system was designed in Ref. [14], incorporating a BESS device to assist the EL in hydrogen production, and the capacity of this system was determined in terms of energy losses and hydrogen production costs. Experimental results showed that the utilization of BESS reduced the required capacity of the EL unit, but it also resulted in increased energy losses. In Ref. [15], the authors proposed an off-grid hydrogen production system comprising a PV system, EL, BESS, and a diesel generator, and evaluated the economic feasibility of the system. In Ref. [16], a subsection bi-objective optimization dynamic programming strategy was proposed for managing a photovoltaic/battery/hydrogen hybrid energy system, aiming to simplify control complexity through rule-based judgment and dynamic programming. Moreover, the renewable energy hydrogen production system can be connected to the utility grid, enabling the transfer of energy between the system and the grid to avoid frequent start-stop operations. This integration allows the grid-connected system to improve its economic efficiency by participating in the electricity market. In Ref. [17], a grid-connected PV hydrogen production system was designed. In this system, when the PV power generation is below or exceeds the safe operating power of the EL unit, the excess electricity will be supplied to the grid. In Ref. [18], an optimal energy scheduling solution for the grid-connected PV hydrogen production system was proposed, and the electricity market was considered to mitigate power fluctuations of the EL unit and reduce the hydrogen production costs.

Renewable power generation is intermittent and variable, and the slow response of EL devices is one of its notable features. Although PEM-EL has a fast response time of a few seconds, it cannot fully adapt to the variability of renewable energy sources. This mismatch can lead to power imbalances and reduce the utilization of renewable energy [19]. Supercapacitors (SC) possess fast response speeds and long service lives, making them capable of frequent and rapid charge and discharge cycles to compensate for power imbalances [20,21]. A control strategy for a wind-hydrogen hybrid power generation system was proposed in Ref. [22]. This strategy utilizes SC to cope with the slow dynamic response characteristics of the EL, ensuring optimal energy management of the power generation system and enhancing system reliability.

To this end, an off-grid PV-based hydrogen production system consisting of PV, EL, BESS and SC units was developed. A coordinated operation strategy is designed to manage the power of each unit in the system to avoid significant fluctuations in working power and frequent start-stop cycles of the EL unit. The proposed coordinated operation strategy sets five operation modes for the PV-based hydrogen production system, and the fuzzy logic control algorithm is used to choose the operation mode to determine the reference power of each unit. On this basis, the state of charge (SOC) feedback-based first-order low-pass filter (FLF) algorithm is used to achieve the power allocation to mitigate deep charging and discharging of the SC. The main contributions of this work are summarized as follows.

(1) The coordinated operation solution sets five operation modes for the PV-based hydrogen production system, and the fuzzy logic control algorithm is used to choose the operation mode to determine the reference power of each unit.
(2) A SOC feedback-based first-order low-pass filter algorithm is used for power allocation, effectively mitigating deep charging and discharging of the SC.
(3) The proposed solution was evaluated by conducting simulations on three typical test days and compared against a benchmark solution. Numerical results confirm the effectiveness of the proposed coordinated operation strategy, demonstrating its ability to effectively prevent frequent start-stop cycles of the EL units.

The rest of the paper is organized as follows: Section II introduces the modeling of the off-grid PV hydrogen production system. Section III presents the implementation of the proposed coordinated operation

solution. A performance evaluation of the solution is presented in Section IV and Section V concludes the paper.

## 2. System model

The PV hydrogen production system developed in this work consists of a PV system, EL, BESS and SC unit. The framework for PV-based hydrogen production system is shown in Fig. 1. BESS have a large capacity but exhibit a low response speed, and their service life may be reduced by frequent charging and discharging. While SC has the characteristics of fast response speed and long service life, enabling frequent and fast charge and discharge. However, SCs have limited capacity and are not suitable for high-power control tasks. After the hydrogen is produced in the EL, it is stored in the hydrogen storage tank. When the hydrogen storage tank is nearly full, the hydrogen is sold to the hydrogen market.

EL units can consume electricity to produce hydrogen via water electrolysis. The hydrogen produced can be expressed by Eq. (1), and Eq. (2) defines the upper and lower limits of the power input of EL equipment.

$$H_{\mathrm{EL}}(t) = P_{\mathrm{EL}}(t) E_{\mathrm{EL}} \eta_{\mathrm{EL}} \tag{1}$$

$$P_{\mathrm{EL}}^{\min} \le P_{\mathrm{EL}}(t) \le P_{\mathrm{EL}}^{\max} \tag{2}$$

where, $H_{\mathrm{EL}}$ and $P_{\mathrm{EL}}$ represent the hydrogen produced and electricity consumed by the EL unit. $P_{\mathrm{EL}}^{\min}$ and $P_{\mathrm{EL}}^{\max}$ represent the lower and upper boundary of the power input of the EL unit, respectively. $E_{\mathrm{EL}}$ is the energy conversion factor and $\eta_{\mathrm{EL}}$ is the efficiency of the EL unit. To simplify modeling, the energy loss of the compressor is included in the efficiency of the EL unit.

The SOC of the energy storage units (containing the BESS and SC unit) at each time slot can be expressed as Eq. (3). The superscripts "type" denotes the energy storage type, i.e., BESS or SC. The SOC limitation can be described as Eq. (4). Two binary variables $I_{type,\mathrm{ch}}$ and $I_{type,\mathrm{disc}}$ are introduced to prevent simultaneous charging and discharging of the BESS and SC, which can be defined in Eq. (5). Eqs. (6) and (7) denote the charging and discharging power limitations of the BESS and the SC, respectively.

$$SOC_{type}(t) = SOC_{type}(t-1) + \frac{\left(P_{type,\mathrm{ch}}(t)\eta_{type,\mathrm{ch}} - P_{type,\mathrm{disc}}(t)/\eta_{type,\mathrm{disc}}\right)}{C_{type}}\Delta t \tag{3}$$

$$SOC_{type}^{\min} \le SOC_{type}(t) \le SOC_{type}^{\max} \tag{4}$$

$$I_{type,\mathrm{ch}}(t) + I_{type,\mathrm{disc}}(t) \le 1 \tag{5}$$

$$0 \le P_{type,\mathrm{ch}}(t) \le P_{type,\mathrm{ch}}^{\max} I_{type,\mathrm{ch}}(t) \tag{6}$$

$$0 \le P_{type,\mathrm{disc}}(t) \le P_{type,\mathrm{disc}}^{\max} I_{type,\mathrm{disc}}(t) \tag{7}$$

where $P_{type,\mathrm{ch}}$ and $P_{type,\mathrm{disc}}$ denote the charging and discharging power. $\eta_{type,\mathrm{ch}}$ and $\eta_{type,\mathrm{disc}}$ are the efficiency of the power charging and discharging. $C_{type}$ is the energy storage capacity; $SOC_{type}^{\min}$ and $SOC_{type}^{\max}$ denote the upper and lower limit of the SOC value, $P_{type,\mathrm{ch}}^{\max}$ and $P_{type,\mathrm{disc}}^{\max}$ denotes the maximum power charging/discharging power.

## 3. Coordinated operation solution

Due to the high randomness and volatility of PV power generation, a sampling period of 1 s was chosen for the applications. However, the utilization of short-term forecasting of PV power output in real-time power management is limited due to inherent errors. Moreover, compared to optimization-based methods, the fuzzy logic method is particularly advantageous for real-time control systems as it facilitates quicker decision-making by eliminating the need to solve complex optimization problems. Consequently, the coordinated operation strategy for the PV hydrogen production system designed in this work does not involve short-term forecasting and intelligent optimization algorithms.

The proposed coordinated operation solution designed five operating modes for the PV hydrogen production system, and a fuzzy logic control algorithm is employed to determine the reference power instructions for the EL and the BESS unit in each time slot. These reference power instructions indicate target operating power the EL and the BESS. Then, the SOC feedback-based FLF algorithm is utilized to allocate power among the EL, BESS and SC units. The SOC feedback strategy is implemented to adaptively adjust the filtering coefficients of the FLF algorithm based on the SOC value of SC, thereby mitigating deep charging and discharging of the SC. This coordinated operation strategy considers the operational characteristics, response abilities and factors impacting the degradation of the EL, which improves the operational efficiency of the PV hydrogen production system. The flowchart of the coordinated operation solution for the PV hydrogen production system is illustrated in Fig. 2.

### 3.1. Operating mode

The SOC value of BESS in the previous time slot and the PV output in the current time slot are taken as the input of the fuzzy logic system for determining the operation mode of the PV hydrogen system. Thus, the reference power instructions for the EL and the BESS in the current time

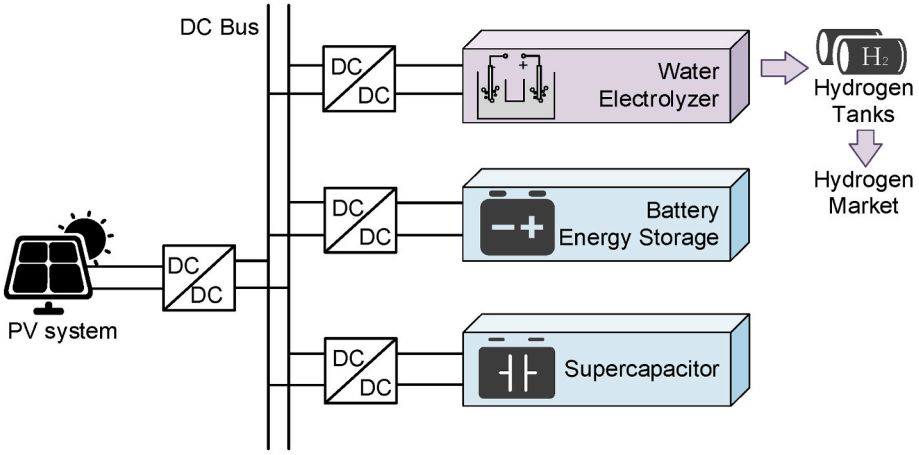


**Fig. 1.** Operation framework for PV-based hydrogen production system.

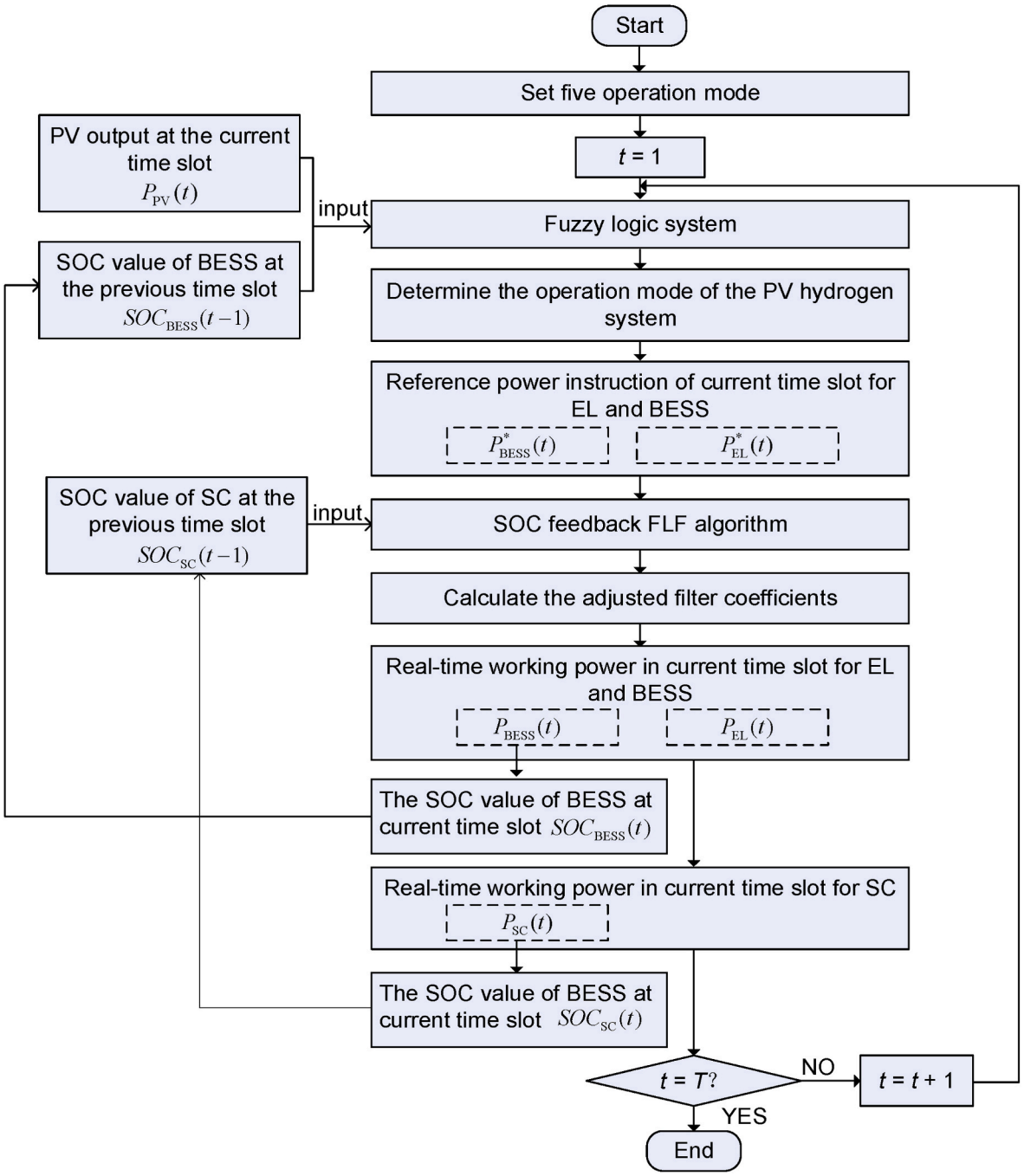


**Fig. 2.** Flowchart of coordinated operation solution for PV hydrogen production system.

slot are obtained.

The operation modes of the PV hydrogen production system comprise five modes, which are as follows.

1) MODE 1

In MODE 1, the power generated by the PV system is absorbed by the BESS, while the EL remains deactivated, which can be expressed as,

$$\begin{cases} P^*_{EL}(t) = 0 \\ P^*_{BESS}(t) = P_{PV}(t) \end{cases} \tag{8}$$

where, the reference power instructions, $P^*_{EL}$ and $P^*_{BESS}$, serve as the targeted power outputs for the EL and the BESS, respectively.

2) MODE 2

In MODE 2, the BESS cooperates with PV power generation to supply power to the EL, and the EL operates at the minimum input power. This can be illustrated as,

$$\begin{cases} P^*_{EL}(t) = P^{min}_{EL} \\ P^*_{BESS}(t) = P_{PV}(t) - P^{min}_{EL} \end{cases} \tag{9}$$

3) MODE 3

In MODE 3, the BESS collaborates with the PV system to provide power to the EL, and the input power of the EL remains consistent with the previous moment. This can be represented as,

$$\begin{cases} P^*_{\mathrm{EL}}(t) = P_{\mathrm{EL}}(t-1) \\ P^*_{\mathrm{BESS}}(t) = P_{\mathrm{PV}}(t) - P^*_{\mathrm{EL}}(t) \end{cases} \tag{10}$$

4) MODE 4

In MODE 4, the power generated by the PV system supplies to the EL, while the battery remains inactive, which can be expressed as,

$$\begin{cases} P^*_{\mathrm{EL}}(t) = P_{\mathrm{PV}}(t) \\ P^*_{\mathrm{BESS}}(t) = 0 \end{cases} \tag{11}$$

5) MODE 5

In MODE 5, the EL operates at the maximum input power, and the remaining output power from the PV system is stored in the battery. This can be illustrated as,

$$\begin{cases} P^*_{\mathrm{EL}}(t) = P^{\max}_{\mathrm{EL}} \\ P^*_{\mathrm{BESS}}(t) = P_{\mathrm{PV}}(t) - P^{\max}_{\mathrm{EL}} \end{cases} \tag{12}$$

### 3.2. Fuzzy control-based operation mode selection

In a fuzzy control system, input and output variables are subjected to fuzzy processing, and membership degrees are assigned to these variables [23]. In this work, the operating power range of the EL is set from 1 kW to 10 kW, and the description of two inputs and one output for the fuzzy control system are as follows:

Input 1: the SOC value of BESS at the previous time slot, i.e., $SOC_{\mathrm{BESS}}(t-1)$. Its range is [0.2,0.8], which reflects the remaining capacity of the battery, and its fuzzy set can be expressed as {VS, S, M, B, VB} (where VS represents very small, S represents small, M represents medium, B represents large, and VB represents very large). The membership functions for *SOC* are shown in Fig. 3.

Input 2: The current PV output power $P_{\mathrm{PV}}(t)$. Its range is [0,20 kW], and its fuzzy set can be expressed as {VS, S, M, B, VB}. The membership functions for PV power generation are shown in Fig. 4.

Output: System operation mode. It will choose one of the five modes depending on the result of the fuzzification of input 1 and input 2, and its fuzzy set can be expressed as {MODE 1, MODE 2, MODE 3, MODE 4, MODE 5}. The membership functions for the system operation mode are shown in Fig. 5.

In this fuzzy control system, there are two fuzzy logic control rules: A and B, as illustrated in Tables 1 and 2, respectively. If the current PV power generation is greater than the operating power of the EL in the previous time slot, i.e., $P_{\mathrm{PV}}(t) > P_{\mathrm{EL}}(t-1)$, fuzzy control rule A is applied. Otherwise, i.e., $P_{\mathrm{PV}}(t) \le P_{\mathrm{EL}}(t-1)$, fuzzy control rule B is applied.

When the current PV power generation is greater than the operating power of the EL in the previous time slot, the selection of operating modes proceeds as follows. If both the SOC of the BESS and the PV

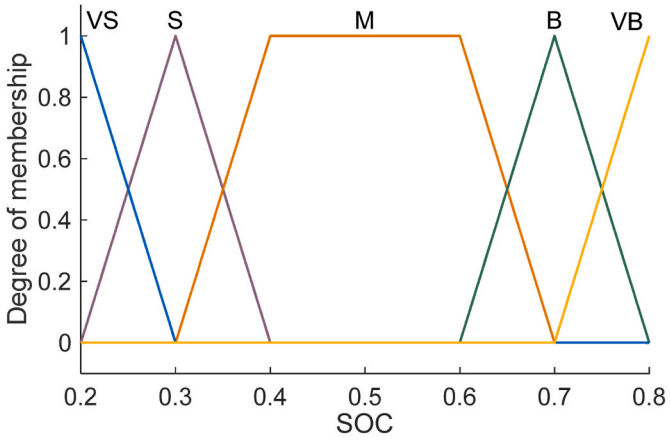


**Fig. 3.** Membership function of SOC value of BESS.

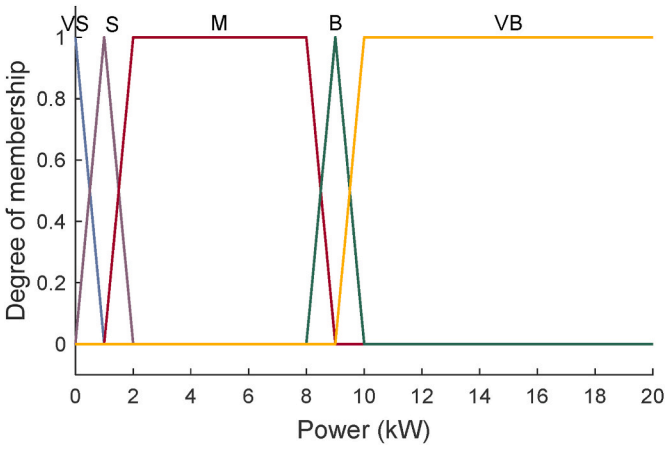


**Fig. 4.** Membership function of PV power generation.

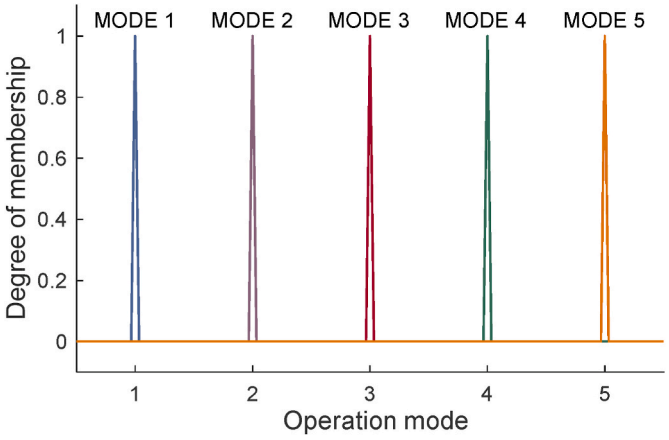


**Fig. 5.** Membership function of the operating mode.

**Table 1**
Fuzzy logic control rule A.

| Operation mode | | $SOC_{\mathrm{BESS}}(t-1)$ | | | | |
|---|---|---|---|---|---|---|
| | | VS | S | M | B | VB |
| $P_{\mathrm{PV}}(t)$ | VS | MODE 3 | MODE 3 | MODE 2 | MODE 2 | MODE 2 |
| | S | MODE 3 | MODE 3 | MODE 3 | MODE 2 | MODE 2 |
| | M | MODE 3 | MODE 4 | MODE 4 | MODE 4 | MODE 4 |
| | B | MODE 3 | MODE 4 | MODE 5 | MODE 5 | MODE 5 |
| | VB | MODE 5 | MODE 5 | MODE 5 | MODE 5 | MODE 5 |

**Table 2**
Fuzzy logic control rule B.

| Operation mode | | $SOC_{\mathrm{BESS}}(t-1)$ | | | | |
|---|---|---|---|---|---|---|
| | | VS | S | M | B | VB |
| $P_{\mathrm{PV}}(t)$ | VS | MODE 1 | MODE 3 | MODE 3 | MODE 3 | MODE 3 |
| | S | MODE 1 | MODE 3 | MODE 3 | MODE 3 | MODE 3 |
| | M | MODE 4 | MODE 4 | MODE 3 | MODE 3 | MODE 3 |
| | B | MODE 4 | MODE 4 | MODE 3 | MODE 3 | MODE 3 |
| | VB | MODE 5 | MODE 5 | MODE 5 | MODE 5 | MODE 5 |

output are relatively low, MODE 3 is typically chosen, where the EL maintains the same input power as previous moment and any excess electricity is stored in the BESS. If the SOC is high while the PV output remains low, MODE 2 is selected, where the BESS and the PV system work together to power the EL, ensuring it operates at least at its minimum working power. When there is available charge in the BESS and the PV output is sufficient but not excessive, MODE 4 is chosen, allowing the PV system to directly power the EL. As the PV output gradually increases, the system shifts to MODE 5, where the EL operates at its maximum input power. If the PV output is insufficient, the BESS discharges to supplement it; if there is surplus power, it is stored in the BESS.

When the current PV power generation is less than the operating power of the EL in the previous time slot, the selection of operating modes proceeds as follows. If the PV output is extremely low, MODE 1 is chosen, deactivating the EL and storing all generated electricity in the BESS. If the BESS's SOC is low while the PV output meets the EL's operational power requirements, MODE 4 is selected, allowing the PV system to directly power the EL. When the BESS has available charge and the PV output is sufficient but not excessive, MODE 3 is employed, where both the BESS and PV system collaborate to supply power to the EL, ensuring a stable power input. When the PV output is very high, MODE 5 is activated, allowing the EL to operate at maximum input power, with any excess electricity stored in the BESS.

### 3.3. SOC feedback FLF algorithm

The EL and BESS devices have a slow response time of a few seconds, which limits their ability to fully adapt to the variability of PV power generation. This mismatch can lead to power imbalances and reduce the utilization of renewable energy. SC possess fast response speed, enabling them to perform frequent and rapid charge and discharge cycles to compensate for power imbalances.

A SOC feedback FLF algorithm is proposed in this work to determine the power values of EL, BESS and SC. The FLF algorithm is utilized to achieve the power allocation, and the control diagram is depicted in Fig. 6. This algorithm divides the input reference power into two components, i.e., the low-frequency power component and the high-frequency power component. The low-frequency power component exhibits slower fluctuation speeds, and this portion of power is assumed by the BESS and EL. The high-frequency power component, characterized by rapid variations, requires a quick response from the energy storage medium. It is allocated to the SC to compensate for the imbalanced power in the slower dynamic response of the BESS and EL unit. Further, in this algorithm, the SOC of SC at the previous time slot is used to determine the accommodation coefficient ($F$), and adaptively adjusts the filtering coefficient $a$ and $b$ to avoid deep charging and discharging of the SC.

The FLF algorithm is mainly derived from the principle of the FLF filter, and the circuit structure is shown in Fig. 7. In the figure, $U_i$ is the input signal, $U_0$ is the filtered output signal, $R$ is the filtering resistance, and $C$ is the filtering capacitance.

Based on the input-output relationship of the FLF filter circuit, the mathematical model can be expressed as,

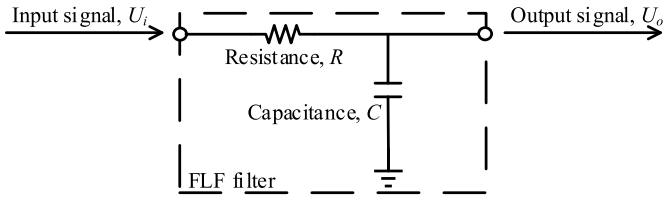


**Fig. 7.** The circuit diagram of a FLF filter.

$$\tau\frac{dU_o}{dt}+U_o=U_i \tag{13}$$

where $\tau$ is the time constant of the filter, and $\tau = RC$. In practical applications, the output power of PV generation is obtained through sampling, with a sampling period represented by $T_s$. Discretizing Eq. (13) yields Eq. (14) [24].

$$P_o(t)=\frac{T_s}{\tau+T_s}P_i(t)+\frac{\tau}{\tau+T_s}P_o(t-1) \tag{14}$$

where $P_i$ is the input power signal, and $P_o$ is the output power signal after filtering. A filtering coefficient $\alpha$ is redefined to simplify the FLF algorithm, which can be expressed as,

$$\alpha=\frac{T_s}{\tau+T_s} \tag{15}$$

Since the range of $\tau$ is limited to $[0,\infty)$, according to Eq. (16), the range of $\alpha$ can be obtained is $(0,1]$. At this time, the FLF algorithm can be illustrated as,

$$P_o(t)=\alpha P_i(t)+(1-\alpha)P_o(t-1) \tag{16}$$

Based on the reference power instructions for the EL and BESS, i.e., $P^*_{EL}$ and $P^*_{BESS}$, the FLF algorithm is used to determine the power values of the EL, BESS and SC, i.e., $P_{EL}$, $P_{BESS}$ and $P_{SC}$. The specific steps for using the FLF algorithm to calculate are as follows:

Step 1: Extract the low-frequency component and high-frequency component from the reference power instructions for the EL, which can be calculated as,

$$P^*_{EL-L}(t)=aP^*_{EL}(t)+(1-a)P_{EL}(t-1) \tag{17}$$

$$P^*_{EL-H}(t)=P^*_{EL}(t)-P^*_{EL-L}(t) \tag{18}$$

where, $a$ represents the filter coefficient corresponding to the EL. $P^*_{EL-L}$ and $P^*_{EL-H}$ represent the low-frequency and high-frequency component of the reference power instructions for the EL.

Step 2: Extract the low-frequency and high-frequency components from the reference power instructions for the BESS, which can be expressed as,

$$P^*_{BESS-L}(t)=bP^*_{BESS}(t)+(1-b)P_{BESS}(t-1) \tag{19}$$

$$P^*_{BESS-H}(t)=P^*_{BESS}(t)-P^*_{BESS-L}(t) \tag{20}$$

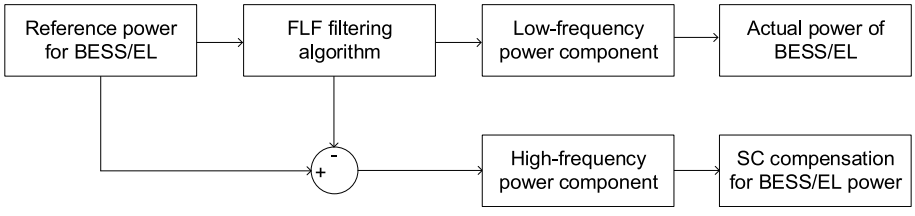


**Fig. 6.** Power allocation based on FLF algorithm.

where, $b$ represents the filter coefficient corresponding to the BESS. $P^{*}_{\mathrm{BESS-L}}$ and $P^{*}_{\mathrm{BESS-H}}$ represent the low-frequency and high-frequency components of the reference power instructions for the BESS.

Step 3: The low-frequency power component of the EL and BESS power instructions corresponds to the real-time working power of the EL and BESS, which can be expressed by,

$$P_{\mathrm{EL}}(t) = P^{*}_{\mathrm{EL-L}}(t) \tag{21}$$

$$P_{\mathrm{BESS}}(t) = P^{*}_{\mathrm{BESS-L}}(t) \tag{22}$$

Step 4: The high-frequency power component of the EL and BESS power instructions is compensated and regulated by the SC, which can be calculated as,

$$P_{\mathrm{SC}}(t) = P^{*}_{\mathrm{EL-H}}(t) + P^{*}_{\mathrm{BESS-H}}(t) \tag{23}$$

Further, the semi-parabolic membership function is used to define $F$, which can be expressed as Eq. (24), and the corresponding relationship between $SOC_{\mathrm{SC}}(t-1)$ and $F$ is shown in Fig. 8.

$$F = \begin{cases} -0.25 \times \left(\dfrac{0.3 - SOC_{\mathrm{SC}}(t-1)}{0.3 - 0.05}\right)^2 + 0.75, \\ \qquad 0.05 \le SOC_{\mathrm{SC}}(t-1) \le 0.3 \\ 0.75, \\ \qquad 0.3 < SOC_{\mathrm{SC}}(t-1) < 0.7 \\ 0.25 \times \left(\dfrac{SOC_{\mathrm{SC}}(t-1) - 0.7}{0.95 - 0.7}\right)^2 + 0.75, \\ \qquad 0.7 \le SOC_{\mathrm{SC}}(t-1) \le 0.95 \end{cases} \tag{24}$$

The adjusted filter coefficients $a$ and $b$ can be calculated as,

$$\begin{cases} a(t) = a^{\max} \times F(t), P_{\mathrm{EL}}(t) > P_{\mathrm{EL}}(t-1) \\ a(t) = a^{\max} \times (1 - F(t)), P_{\mathrm{EL}}(t) < P_{\mathrm{EL}}(t-1) \end{cases} \tag{25}$$

$$\begin{cases} b(t) = b^{\max} \times F(t), P_{\mathrm{BESS}}(t) > P_{\mathrm{BESS}}(t-1) \\ b(t) = b^{\max} \times (1 - F(t)), P_{\mathrm{BESS}}(t) < P_{\mathrm{BESS}}(t-1) \end{cases} \tag{26}$$

where $a^{\max}$ and $b^{\max}$ are the maximum filter coefficients values of EL and BESS, respectively.

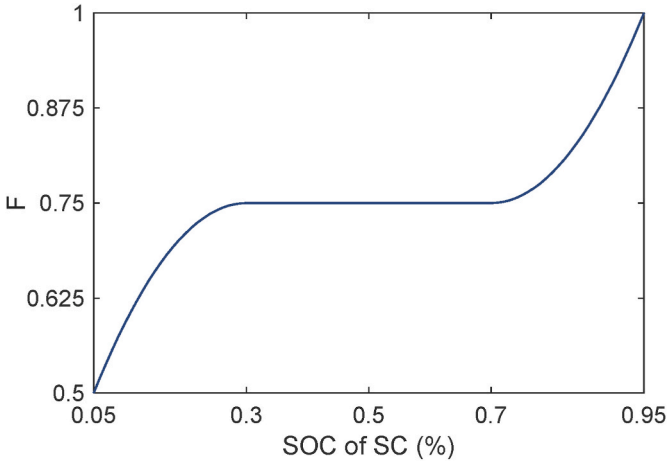


**Fig. 8.** Corresponding relationship between the SOC of SC and the accommodation coefficient.

## 4. Case study

### 4.1. Simulation Setup

To evaluate the performance of the proposed coordinated operation strategy for an off-grid PV hydrogen production system, three typical test cases of sunny, cloudy and rainy days are considered. The PV power generation curves for these conditions are depicted in Fig. 9(a), (b) and (c), respectively. Recent reports suggest that the efficiency of PEM electrolysis is projected to reach 82–86% by 2030 [25]. Moreover, according to Ref. [26], compressors typically operate with an efficiency ranging from 85% to 95%. In the test system, the parameter $\eta_{\mathrm{EL}}$ is set at 80%, which includes the power loss of the hydrogen compressor. The other parameters for the EL, BESS and SC units are given in Table 3 [27–29], and the rated power of the PV system is set as 16 MW. It should be noted that the equipment parameters used here are examples to validate the effectiveness of the proposed method. The coordinated operation strategy proposed was designed to be versatile and adaptable, making it suitable for use with equipment having different parameter configurations. This adaptability ensures that the operation strategy can be effectively applied to a variety of equipment parameters, accommodating changes in technology or different specifications of devices used in the PV hydrogen production systems.

In this study, the response times for the PEM-EL and the BESS are assumed to be 5 s and 3 s, respectively [30,31]. The response is typically considered complete after $5\tau$. According to eq. (15), the maximum filter coefficients value for the EL and BESS, with a sampling time of 1 s, are 0.500 and 0.625 respectively, i.e. $a^{\max} = 0.500$ and $b^{\max} = 0.625$. Moreover, the rule inputs for the fuzzy control system can be obtained by Figss. 3–5.

The programs are performed in Matlab (version 2022b) and executed on a computer equipped with 3.20 GHz AMD Ryzen 7 2700 and 16.0 GB. The sampling interval is 1 s, and the average executive time for each time slot decision is $5.32 \times 10^{-4}$ s. This means that the proposed coordinated operation solution for the PV hydrogen production system can be implemented in a real-time fashion.

### 4.2. Simulation results

#### 4.2.1. Test case 1: sunny day

In test case 1, the coordinated operation results and the system operation mode are depicted in Fig. 10. The SOC values for the BESS and SC are illustrated in Fig. 12(a) and (b), respectively.

As shown in Fig. 10, during the initial stages of PV operation, the power output is relatively low and is absorbed by the BESS. As the PV power output gradually increases, the EL starts to operate. With fluctuations in the PV output, the BESS collaborates with the PV output fluctuations when there is sufficient remaining energy. When the PV power generation operates at its maximum power, and the remaining PV output is absorbed by the BESS. In the latter half of the day, the PV output gradually decreases below the maximum working power of the EL. By this time, the BESS unit has accumulated a large amount of energy. The BESS collaborates with the PV system to supply power to the EL unit, allowing it to maintain continuous operation at a high power state. Subsequently, when the PV output drops to zero and the SOC value of BESS is low, the EL stops working.

Fig. 11 illustrates the power coordination details in test case 1, with two specific time periods at 8:00:27 and 18:22:48. As shown in Fig. 11 (a), the PV output gradually increases, switching the system from operation mode 3 to operation mode 4, and the EL starts working. At this point, both the reference power of the EL and the BESS have changed. However, their actual power cannot fully keep up with the reference power, resulting in the remaining PV output being absorbed by the SC. In Fig. 11(b), at 18:22:48, the PVoutput power is zero and the remaining energy stored in the BESS is insufficient to support the ELoperation, leading to the system transitioning from operation mode 3 to operation

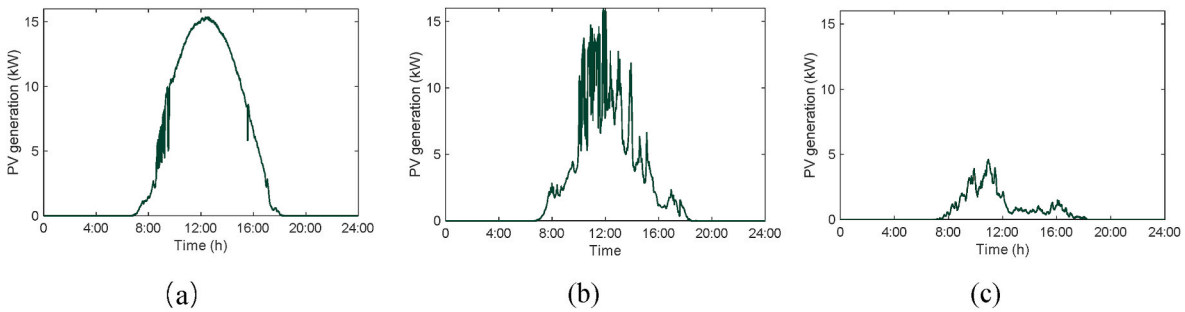


**Fig. 9.** PV curves in (a) test case1, (b) test case 2, and (c) test case 3.

**Table 3**
The required parameters for modeling the system.

| | Parameters | Value |
|---|---|---|
| EL | $P^{max}_{EL}/P^{min}_{EL}$ (kW) | 10/1.0 |
| | $E_{EL}$ (kg/kWh) | 0.025 |
| | $\eta_{EL}$ (%) | 0.8 |
| BESS | $C_{BESS}$ (kWh) | 25 |
| | $P^{max}_{BESS,ch}/P^{max}_{BESS,disc}$ (kW) | 10 |
| | $SOC^{max}_{BESS}/SOC^{min}_{BESS}$ | 0.8/0.2 |
| | $\eta_{BESS,ch}/\eta_{BESS,disc}$ (%) | 0.95/0.95 |
| SC | $C_{SC}$ (kWh) | 0.1 |
| | $P^{max}_{SC,ch}/P^{max}_{SC,disc}$ (kW) | 0.1 |
| | $SOC^{max}_{SC}/SOC^{min}_{SC}$ | 0.95/0.05 |
| | $\eta_{SC,ch}/\eta_{SC,disc}$ (%) | 0.95/0.95 |

mode 1, and causing the EL to shut down.

#### 4.2.2. Test case 2: cloudy day

In test case 2, the coordinated operation results and the system operation mode are depicted in Fig. 13. The SOC values for the BESS and SC are illustrated in Fig. 15(a) and (b), respectively.

As illustrated in Fig. 13, when the PV system becomes active, the BESS absorbs the low PV output power. As the PV output gradually rises, the EL starts operating. However, near the maximum input power of the EL, PV power output experiences significant power fluctuation. In this situation, when the BESS has sufficient energy stored, it provides power to the EL in coordination with the PV. This coordination helps to reduce the fluctuations in the EL input power and mitigate its degradation. Conversely, when the energy stored in the BESS is insufficient, the EL operates in sync with the fluctuating PV output power. Subsequently, as the PV output gradually decreases and fluctuates near the minimum input power of the EL, the sufficient energy stored in BESS allows the EL to operate continuously at its minimum input power.

During this phase, the BESS aims to minimize the number of start-stop operations of the EL, while fully utilizing the PV power generation for hydrogen production.

In this test case, the utilization rate of the SC is notably higher than in test case 1, mainly due to the substantial power fluctuations in the PV output. These fluctuations lead to significant imbalanced power, resulting from the slow responses of the EL and battery energy storage devices.

Fig. 14 presents the power coordination details during the time period around 12:00. In this period, the PV output exhibited fluctuations near the maximum input power of the EL. through the coordinated actions of the BESS and SC, the EL managed to operate consistently at the maximum input power, avoiding frequent power fluctuations. When the PV output declined from above the maximum input power of the EL to below it (e.g., around 11:59), the system transitioned from operation

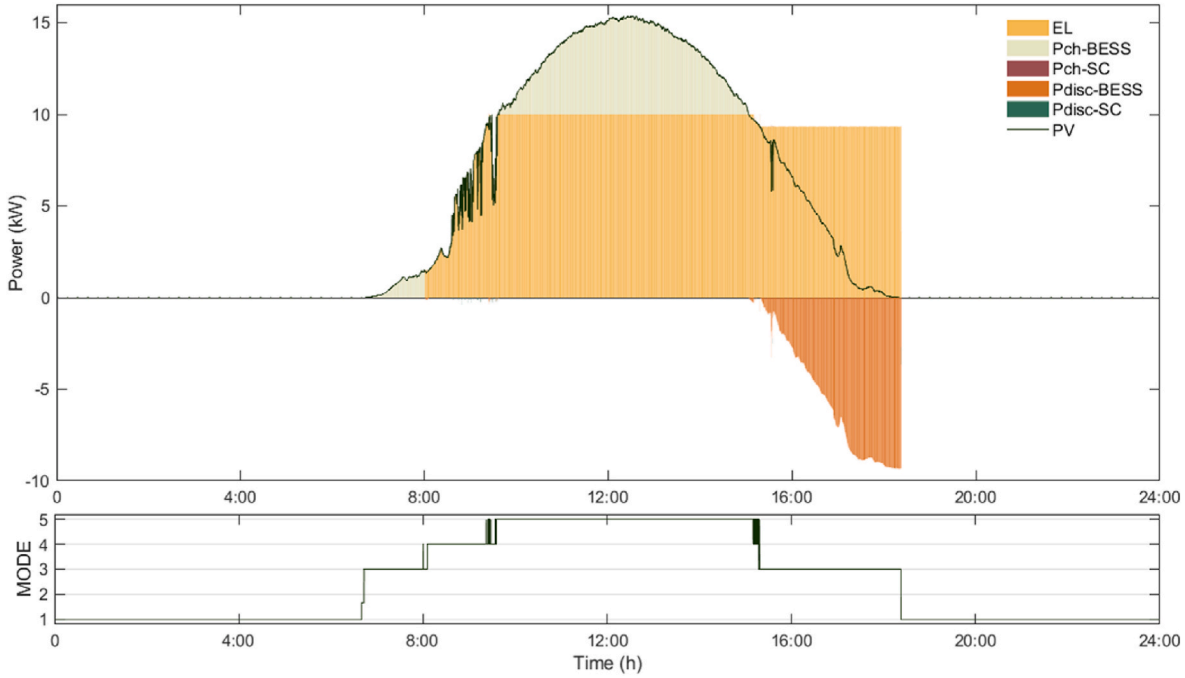


**Fig. 10.** Coordinated operation results and the system operation mode in test case1.

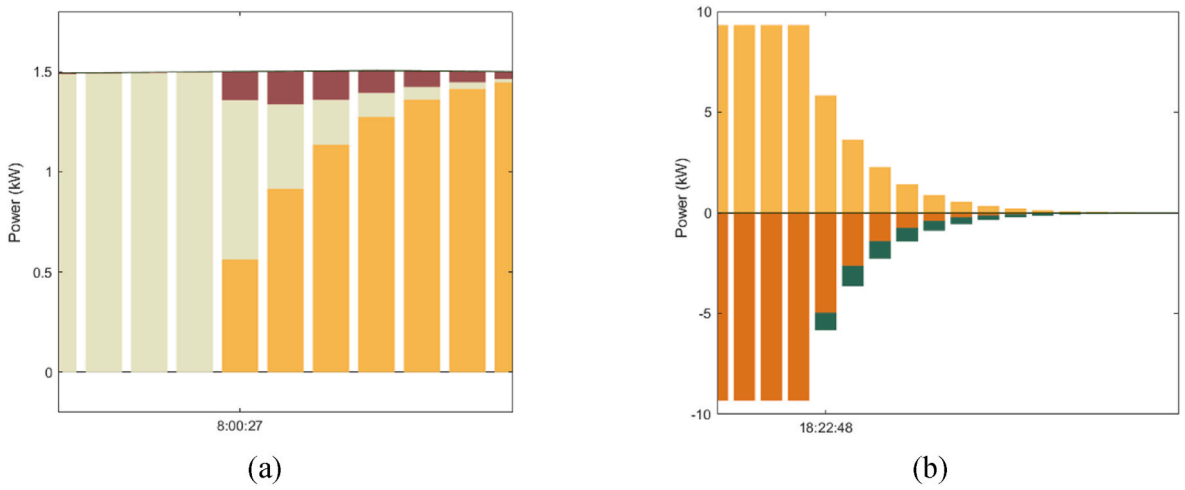


**Fig. 11.** Power synergy detail plot in test case1.

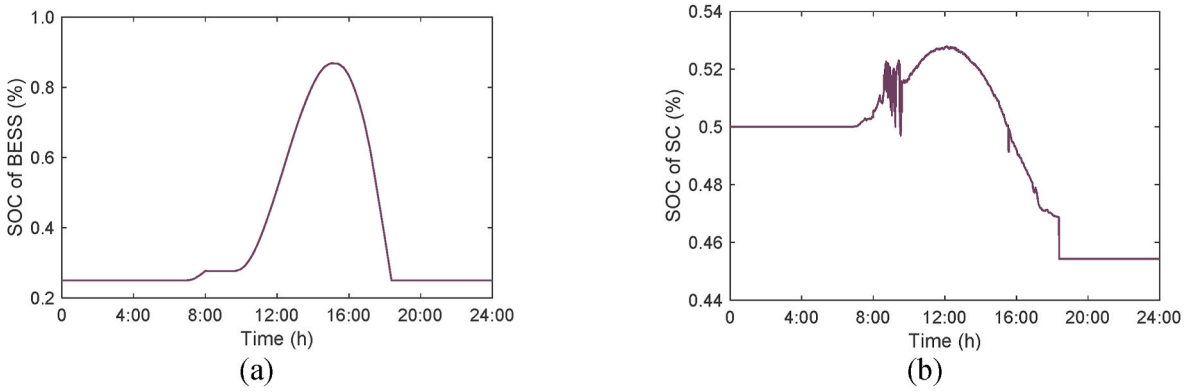


**Fig. 12.** SOC vales for the (a) BESS and (b) SC in test case 1.

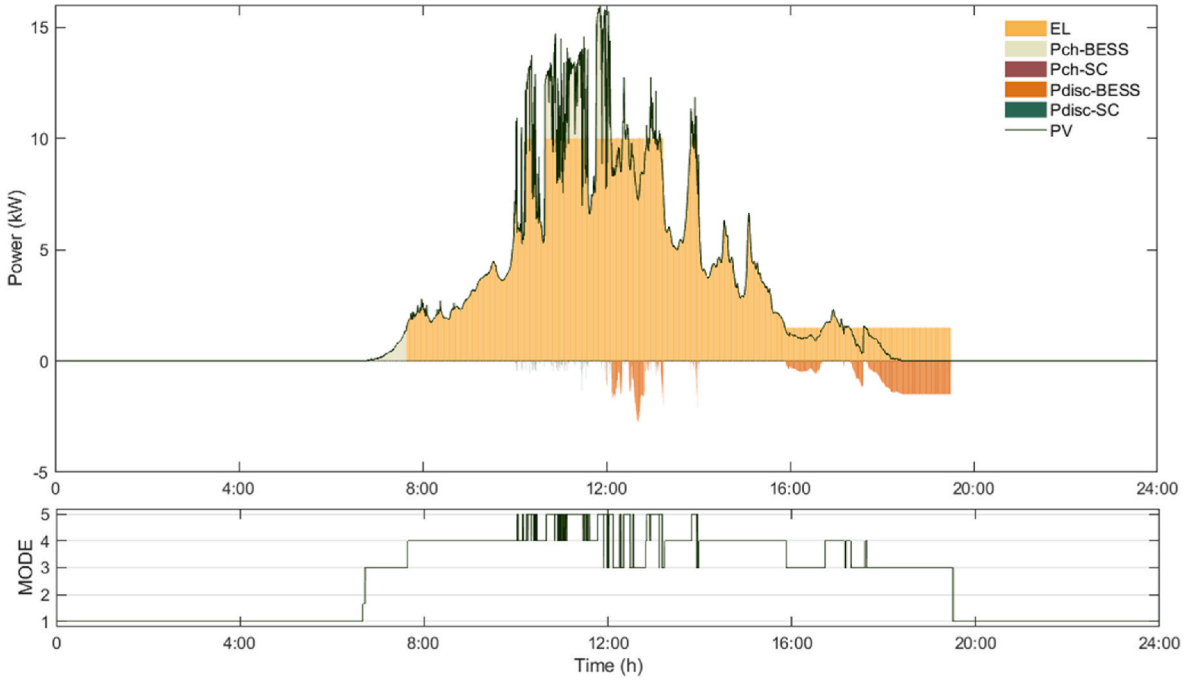


**Fig. 13.** Coordinated operation results and the system operation mode in test case2.

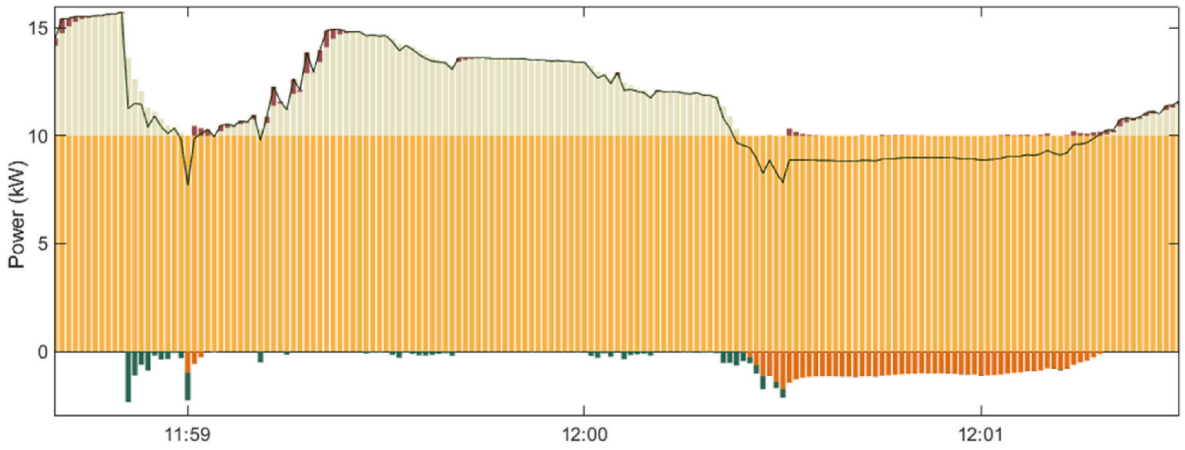


**Fig. 14.** Power synergy detail plot in test case 2.

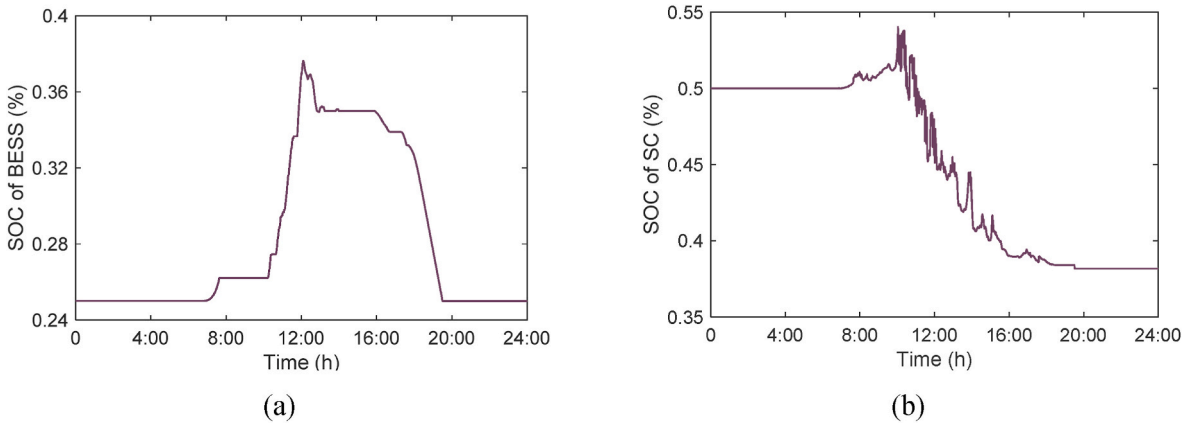


**Fig. 15.** SOC vales for the (a) BESS and (b) SC in test case 2.

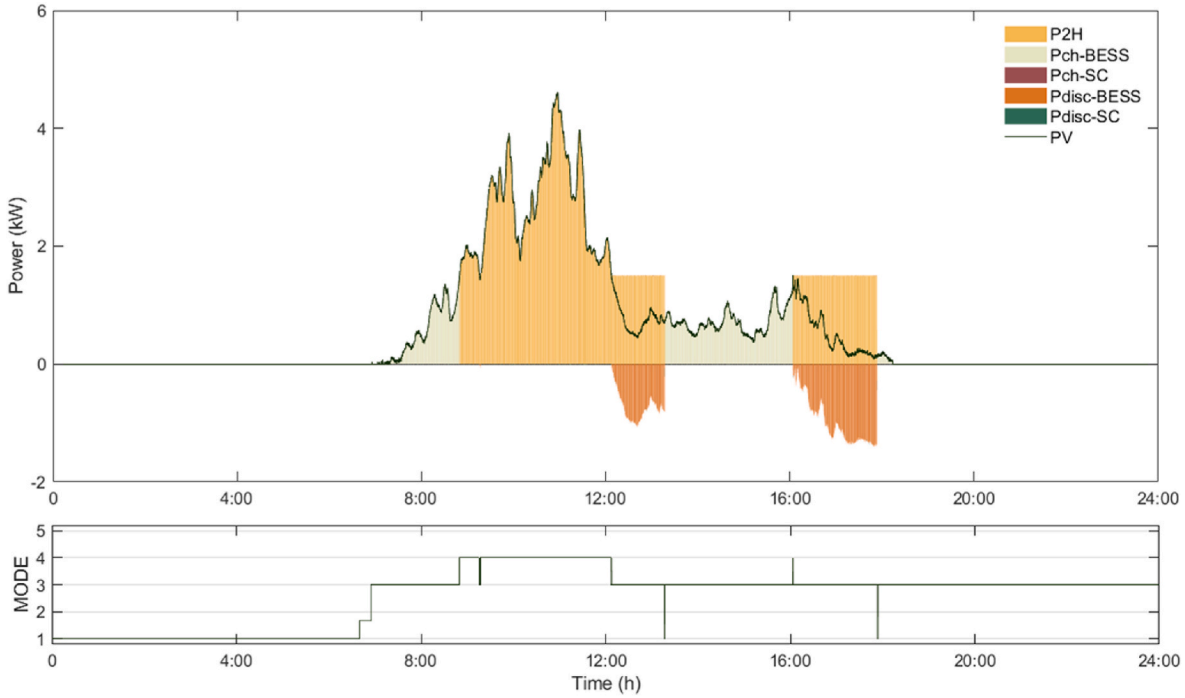


**Fig. 16.** Coordinated operation results and the system operation mode in test case3.

MODE 5 to Operation Mode 3, with BESS discharging power to supply the EL in conjunction with the PV output. From the figure, the coordination between the BESS and SC can be clearly observed. As the BESS discharge power increased, the SC released power to compensate for the imbalance power, and when the BESS discharge power decreased, the SC absorbed power to compensate for the imbalance.

#### 4.2.3. Test case 3: rainy day

In test case 3, the coordinated operation results and the system operation mode are depicted in Fig. 16. Similar to the first two cases, during the initial operation of the PV system, the output power is relatively low, which is absorbed by BESS, and with the gradual increase of PV power generation, EL begins to operate. Subsequently, the PV output gradually decreases below the minimum working power of the EL. The BESS utilizes the surplus power in collaboration with the PV system to enable the EL to operate at the minimum working power. Until the storage value is insufficient, the system switches Mode 3 to Mode 1, resulting in the shutdown of the EL and the absorption of the output from the PV system by the BESS. Then, as the energy stored in the BESS gradually increases, the BESS can collaborate with the PV system to supply power to the EL.

The SOC values for the BESS and SC are presented in Fig. 17(a) and (b), respectively. The PV output does not exceed the maximum input power of the EL, resulting in a limited amount of power for absorption by the BESS. As a result, the SOC of the BESS consistently remains at a low level.

### 4.3. Comparison analysis

Further, to evaluate the performance of the proposed optimal coordinated operation strategy, a benchmark solution is adopted as the comparison: the power management method proposed in Ref. [32]. In this method, the authors have developed a cooperative strategy among PV, EL and BESS, and the specific strategy is outlined as follows.

(1) When the PV output is below the minimum input power of the EL: if the energy stored in the BESS is sufficient to power the EL at the minimum working power for 1 h, the BESS supplies power in conjunction with the PV output to allow the EL to operate; if the energy stored is insufficient, the EL shuts down and the PV output is absorbed by the BESS.
(2) When the PV output is larger than the minimum working power of the EL but less than the maximum input power: the PV output alone powers the EL, and the BESS remains idle.
(3) When the PV output exceeds the maximum input power of the EL: the EL operates at the maximum working power, and the excess PV power output is absorbed by the BESS.

In this work, the hydrogen production and EL degradation costs are selected as indicators for comparative analysis. The hydrogen production of the PV hydrogen production system can be calculated using Eq. (1). The degradation cost of the EL primarily includes the start-stop cost and power fluctuation cost [28,33], which are associated with their start-up and shutdown times and power input fluctuation, and can be calculated as Eq. (27) and Eq. (28):

$$F_{EL}^{on,off} = e_{EL}\left(\sigma_{EL}^{on} + \sigma_{EL}^{off}\right) \tag{27}$$

$$F_{EL}^{Flu} = d_{EL}\Delta P_{EL}(t) \tag{28}$$

where $\sigma_{EL}^{on}$ and $\sigma_{EL}^{off}$ represent the number of start-up/shutdown times of the EL unit during a day, $\Delta P_{EL}$ is the power fluctuation of the EL unit, $e_{EL}$ and $d_{EL}$ are the coefficients of EL start-stop cost and power fluctuation cost, $e_{EL} = 0.004$ \$ and $d_{EL} = 0.0004$ \$/$kW$ [28].

Table 4 presents the hydrogen production volume, start-stop cost and power fluctuation cost of EL. From the table, the hydrogen production volumes in three typical test cases exceed the benchmark, and the total degradation cost (comprising start-stop and power fluctuation costs) is lower than the benchmark. In test case 1 and test case 3, the start-stop cost of EL is much lower than the benchmark. This is because when the PV power fluctuates at the minimum working power of EL, it is easy to start and stop frequently using the benchmark scheme. This demonstrates the effectiveness of the proposed coordinated operation strategy, as they can effectively avoid frequent start-stop of EL unit.

### 4.4. Discussion of SOC feedback FLF method

In test case 2, the initial SOC value of the SC is set at 0.2 to verify the effectiveness of the SOC feedback strategy. The SOC value of SC with and without SOC feedback strategy are depicted in Figs. 18 and 19, respectively. By implementing the proposed SOC feedback, the SOC value of the SC unit at the end of the day reaches approximately 0.19, whereas, without the SOC feedback strategy, the SOC value at the end of the day is around 0.08. This indicated that the proposed SOC feedback strategies can significantly avoid deep charging and discharging of the SC while ensuring the power balance in the off-grid PV hydrogen production system.

## 5. Conclusion

In this work, a coordinated operation solution is proposed to effectively manage the power allocation among the EL, BESS and SC units in the PV-based hydrogen production system, to avoid significant fluctuations in input power and minimize the frequency of start-stop operations of the EL unit. Firstly, the solution sets five operating modes for

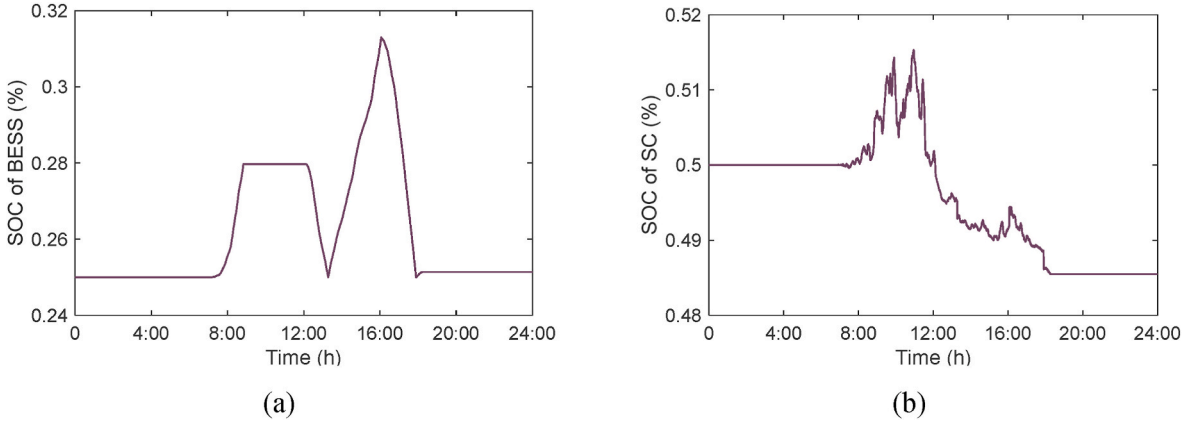


**Fig. 17.** SOC vales for the (a) BESS and (b) SC in test case 3.

**Table 4**
The comparison results.

| | Hydrogen production (kg) | | Start-stop cost of EL ($) | | Fluctuation cost of EL ($) | |
|---|---|---|---|---|---|---|
| | Benchmark | This work | Benchmark | This work | Benchmark | This work |
| Test case 1 | 1.6573 | 1.8729 | 0.028 | 0.008 | 0.0109 | 0.0221 |
| Test case 2 | 1.1010 | 1.1023 | 0.008 | 0.008 | 0.0357 | 0.0147 |
| Test case 3 | 0.2640 | 0.2687 | 0.128 | 0.016 | 0.0090 | 0.0009 |

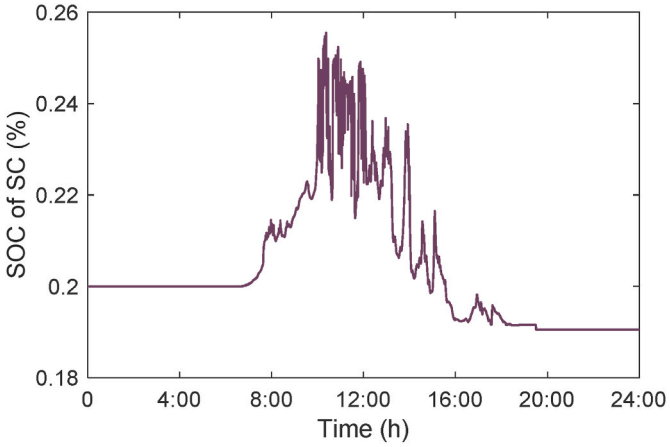


**Fig. 18.** SOC value of SC with SOC feedback over a day.

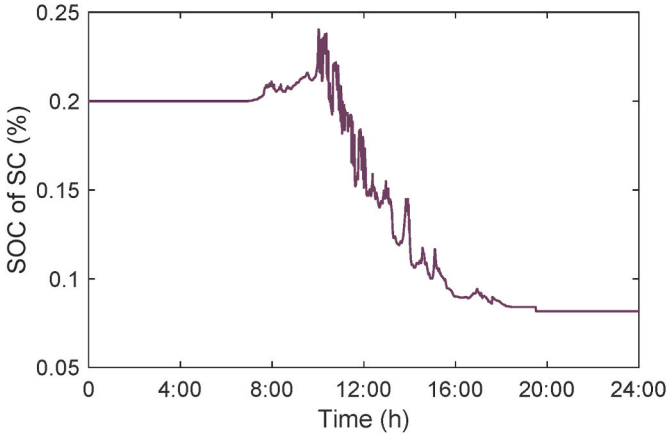


**Fig. 19.** SOC value of SC over a day without SOC feedback off-grid PV hydrogen system.

system. A fuzzy logic control algorithm is employed to select the system operation mode, which determines the reference power for each unit based on the PV output power and the SOC value of the BESS at the previous time slot. Then, a SOC feedback-based FLF algorithm is utilized for power allocation to prevent deep charge/discharge of the SC. To evaluate the performance of the proposed coordinated operation strategy, three typical test cases representing sunny, cloudy, and rainy days were analyzed. Through further comparative analysis of three test cases, numerical results demonstrate that the proposed coordinated operation solution can effectively adjust the system operating mode and outperforms the benchmark solution. Specifically, it achieved a 7.33% increase in mean daily hydrogen production and a 68.26% reduction in degradation costs, demonstrating its effectiveness and superiority in enhancing operational efficiency and sustainability.

In this work, to simplify modeling, the loss of the compressor is included in the efficiency of the EL unit. In fact, the energy consumption of a hydrogen compressor is related to the compression ratio and the intake volume, and the compression ratio changes with variations in the inlet and outlet pressures of the compressor. Given these complexities, the nonlinear model of the compressor needs to be further investigated in future work.

## CRediT authorship contribution statement

**Xiaolun Fang:** Writing – review & editing, Writing – original draft. **Xinyu Zhong:** Writing – original draft. **Wei Dong:** Visualization, Funding acquisition. **Fan Zhang:** Visualization, Supervision. **Qiang Yang:** Data curation, Conceptualization.

## Declaration of competing interest

The authors declare that they have no known competing financial interests or personal relationships that could have appeared to influence the work reported in this paper.

## Acknowledgments s

This work was supported by the Key Research and Development Program of Zhejiang Province (2024C01018), Fundamental Research Funds for the Provincial Universities of Zhejiang (GK239909299001-306).

## References

[1] Tao Y, Qiu J, Lai S, Sun X. Coordinated planning of electricity and hydrogen networks with hydrogen supply chain for fuel cell electric vehicles. IEEE Trans Sustain Energy 2023;14(2):1010–23.
[2] Nguyen T, Abdin Z, Holm T, et al. Grid-connected hydrogen production via large-scale water electrolysis. Energy Convers Manag 2019;200:112108.
[3] Fang X, Dong W, Wang Y, Yang Q. Multiple time-scale energy management strategy for a hydrogen-based multi-energy microgrid. Appl Energy 2022;328:120195.
[4] Salehmin MNI, Husaini T, Goh J, Sulong AB. High-pressure PEM water electrolyser: a review on challenges and mitigation strategies towards green and low-cost hydrogen production. Energy Convers Manag 2022;268:1159855.
[5] de Fátima Palhares DDA, Vieira LGM, Damasceno JJR. Hydrogen production by a low-cost electrolyzer developed through the combination of alkaline water electrolysis and solar energy use. Int J Hydrogen Energy 2018;43(9):4265–75.
[6] Cai X, Lin R, Xu J, Lu Y. Construction and analysis of photovoltaic directly coupled conditions in PEM electrolyzer. Int J Hydrogen Energy 2022;47(10):6494–507.
[7] Kovac A, Marcius D, Budin L. Solar hydrogen production via alkaline water electrolysis. Int J Hydrogen Energy 2019;44:9841–8.
[8] Khalilnejad A, Riahy GH. A hybrid wind-PV system performance investigation for the purpose of maximum hydrogen production and storage using advanced alkaline electrolyzer. Energy Convers Manag 2014;80:398–406.
[9] Gallardo F, García J, Ferrario AM, et al. Assessing sizing optimality of OFF-GRID AC-linked solar PV-PEM systems for hydrogen production. Int J Hydrogen Energy 2022;47(64):27303–25.
[10] Benghanem M, Chettibi N, Mellit A, et al. Type-2 fuzzy-logic based control of photovoltaic-hydrogen production systems. Int J Hydrogen Energy 2023;48(91):35477–92.
[11] Garcia-Torres F, Bordons C, Tobajas J, et al. Stochastic optimization of microgrids with hybrid energy storage systems for grid flexibility services considering energy forecast uncertainties. IEEE Trans Power Syst 2021;36(6):5537–47.
[12] Marocco P, Gandiglio M, Santarelli M. Optimal design of PV-based grid-connected hydrogen production systems. J Clean Prod 2024;434:140007.
[13] Dursun E, Acarkan B, Kilic O. Modeling of hydrogen production with a stand-alone renewable hybrid power system. Int J Hydrogen Energy 2012;37:3098–107.
[14] Gutierrez-Martkin F, Amodio L, Pagano M. Hydrogen production by water electrolysis and offgrid solar PV. Int J Hydrogen Energy 2021;46:29038–48.
[15] Gracia L, Casero P, Bourasseau C, et al. Use of hydrogen in off-grid locations, a techno-economic assessment. Energies 2018;11(11):3141.
[16] Huangfu Y, Tian C, Zhuo S, Xu L, Li P, Quan S, Zhang Y, Ma R. An optimal energy management strategy with subsection bi-objective optimization dynamic

programming for photovoltaic/battery/hydrogen hybrid energy system. Int J Hydrogen Energy 2023;48(8):3154–70.
[17] Tebibel H, Medjebour R. Comparative performance analysis of grid connected PV system for H2 production using PEM water, methanol & hybrid sulfur electrolysis. Int J Hydrogen Energy 2018;43:3482–98.
[18] Matute G, Yusta JM, Beyza J, et al. Optimal dispatch model for PVelectrolysis plants in self-consumption regime to produce green hydrogen: a Spanish case study. Int J Hydrogen Energy 2022;47:25202–13.
[19] He Y, Guo S, Dong P, et al. Techno-economic comparison of different hybrid energy storage systems for off-grid renewable energy applications based on a novel probabilistic reliability index. Appl Energy 2022;328:120225.
[20] Abdalla AA, Moursi MSE, El-Fouly TH, Hosani KHA. A novel adaptive power smoothing approach for PV power plant with hybrid energy storage system. IEEE Trans Sustain Energy 2023;14(3):1457–73.
[21] Xiong R, Duan Y, Cao J, Yu Q. Battery and ultracapacitor in-the-loop approach to validate a real-time power management method for an all-climate electric vehicle. Appl Energy 2018;217:153–65.
[22] Abdelkafi A, Krichen L. Energy management optimization of a hybrid power production unit based renewable energies – ScienceDirect. Int J Electr Power Energy Syst 2014;62(11):1–9.
[23] Zhu Y, Wang Z, Guo X, Wei Z. An improved kinetic energy control strategy for power smoothing of PMSG-WECS based on low pass filter and fuzzy logic controller. Elec Power Syst Res 2023;214:108816.
[24] Zhou Y, Yan Z, Li N. A novel state of charge feedback strategy in wind power smoothing based on short-term forecast and scenario analysis. IEEE Trans Sustain Energy 2017;8(2):870–9.
[25] Wikipedia, Proton exchange membrane electrolysis. Available: https://en.wikipedia.org/wiki/Proton_exchange_membrane_electrolysis.
[26] Mohammad-Reza T. Recent advances in hydrogen compressors for use in large-scale renewable energy integration. Int J Hydrogen Energy 2022;47(83):35275–92.
[27] Konstantinopoulos SA, Anastasiadis AG, Vokas GA, et al. Optimal management of hydrogen storage in stochastic smart microgrid operation. Int J Hydrogen Energy 2017;43(1):490–9.
[28] Garcia-Torres F, Vilaplana DG, Bordons C, et al. Optimal management of microgrids with external agents including battery/fuel cell electric vehicles. IEEE Trans Smart Grid 2018;10(4):4299–308.
[29] Li S, Zhu J, Dong H, et al. A novel rolling optimization strategy considering grid-connected power fluctuations smoothing for renewable energy microgrids. Appl Energy 2022;309:118441.
[30] Maroufmashat A, Fowler M. Transition of future energy system infrastructure; through power-to-gas pathways. Energies 2017;10:2–22.
[31] Amin Bambang RT, Rohman AS, et al. Energy management of fuel cell/battery/supercapacitor hybrid power sources using model predictive control. IEEE Trans Ind Inf 2014;10(4):1992–2002.
[32] Tebibel H. Off grid PV system for hydrogen production using PEM methanol electrolysis and an optimal management strategy. Int J Hydrogen Energy 2017;42(30):19432–45.
[33] Petrollese M, Valverde L, Cocco D, et al. Real-time integration of optimal generation scheduling with MPC for the energy management of a renewable hydrogen-based microgrid. Appl Energy 2016;166:96–106.